# HOMOLOGY MODELING OF THE ORTHOFLAVIVIRUS NS1 PROTEIN FOR VIRTUAL SCREENING OF POTENTIAL LIGANDS

***A.D. Fomina[1,2], V.A. Palyulin[2], D.I. Osolodkin[1,3]****

[1]Chumakov Federal Scientific Center for Research and Development
of Immune-and-Biological Products of Russian Academy of Sciences (Institute of Poliomyelitis),
premises 8, bldg. 1, Village of Institute of Poliomyelitis, Settlement Moskovskiy, Moscow, 108819 Russia;
*e-mail: osolodkin_di@chumakovs.su
[2]Department of Chemistry, Lomonosov Moscow State University, Moscow, Russia
[3]Institute of Translational Medicine and Biotechnology,
Sechenov First Moscow State Medical University, Moscow, Russia

The orthoflavivirus NS1 protein is a relatively understudied target for the design of broad-spectrum anti-orthoflaviviral drugs. Currently, the NS1 protein structures of tick-borne orthoflaviviruses have not been published yet, but these structures can be modelled by homology, thus generating a large amount of structural data. We performed homology modelling of the NS1 protein structures of epidemiologically significant orthoflaviviruses and analysed the possibility of using these models in ensemble docking-based virtual screening. The limitations of the method and the importance of separating the models based on the vector organism when selecting an ensemble have been demonstrated.

**Key words:** orthoflaviviruses; NS1 protein; ensemble docking; homology modeling

**DOI:** 10.18097/PBMC20247006456

## INTRODUCTION

The genus *Orthoflavivirus* includes enveloped viruses transmitted by ticks and mosquitoes [1] — and causing dangerous diseases such as dengue fever, Zika fever, West Nile fever, etc. In Russia and Northern Eurasia, tick-borne encephalitis virus (TBEV) is the most widespread orthoflavivirus. The incidence of tick-borne encephalitis grew from 0.4 cases per 100,000 people in 2015 to 0.7 cases in 2019 and 0.9 cases in 2020 [2]. In Russia, the highest recorded incidence rate was 7.0 per 100,000 population in 1996, but in 2020 it reduced to 0.66 [3]. In addition, due to the expansion of the mosquito habitat, cases of West Nile fever are being recorded in Russia [4]. By 2024, there are no direct-acting antiviral drugs approved for medical use against infections caused by orthoflaviviruses. Vaccines have been developed to prevent infections caused by several orthoflaviviruses (TBEV [5], dengue virus (DENV) [6], yellow fever virus (YFV) [7], Japanese encephalitis virus (JEV) [8]). However, they cannot be used to treat diseases post-onset, do not provide complete protection against infection, and their development and widespread use are complicated by antibody-dependent infection enhancement that at least some orthoflaviviruses (DENV, Zika virus (ZIKV)) exhibit [9, 10]. For example, vaccination against TBEV causes the production of ineffective cross-reactive antibodies upon subsequent vaccination against YFV [11].

The genome of orthoflaviviruses is represented by (+)ssRNA with a length of 10–11 kb [12], which is translated into a polyprotein and processed into three structural and seven non-structural proteins (Fig. 1A). Among them, the non-structural protein NS1 plays an important role in the acute form of diseases by causing endothelial leakage due to interaction with endothelial cells [13, 14] and disruption of the glycocalyx [15]. At the same time, NS1 suppresses the immune response by binding to complement system proteins on the cell surface [16, 17]. The NS1 protein also participates in the viral replicative cycle, stabilizing the invagination of the endoplasmic reticulum membranes and the replicative complex located in them [18, 19]. Small molecules interacting with NS1 can be used as lead compounds for the discovery of anti-orthoflavivirus drugs. Mechanisms of action such as modulation of NS1 binding to membranes or other proteins [20] or inhibition of its dimerization [21–23] have been proposed. However, experimental data on the orthoflavivirus NS1 protein with small molecules have not been published, and this complicates the application of classical methods of structure-based ligand design.

However, the apo form structure of the NS1 protein of mosquito-borne orthoflaviviruses has been studied by X-ray crystallography and cryo-electron microscopy (cryo-EM) (Table 1, Supplementary Materials, Table ST1). According to the PDB data, the orthoflavivirus NS1 protein is a glycoprotein consisting of 352 amino acid residues. The molecular weight of the monomer is 48–50 kDa depending on the amino acid sequence and a glycosylation state. At different stages of infection, different multimeric states of NS1 predominate

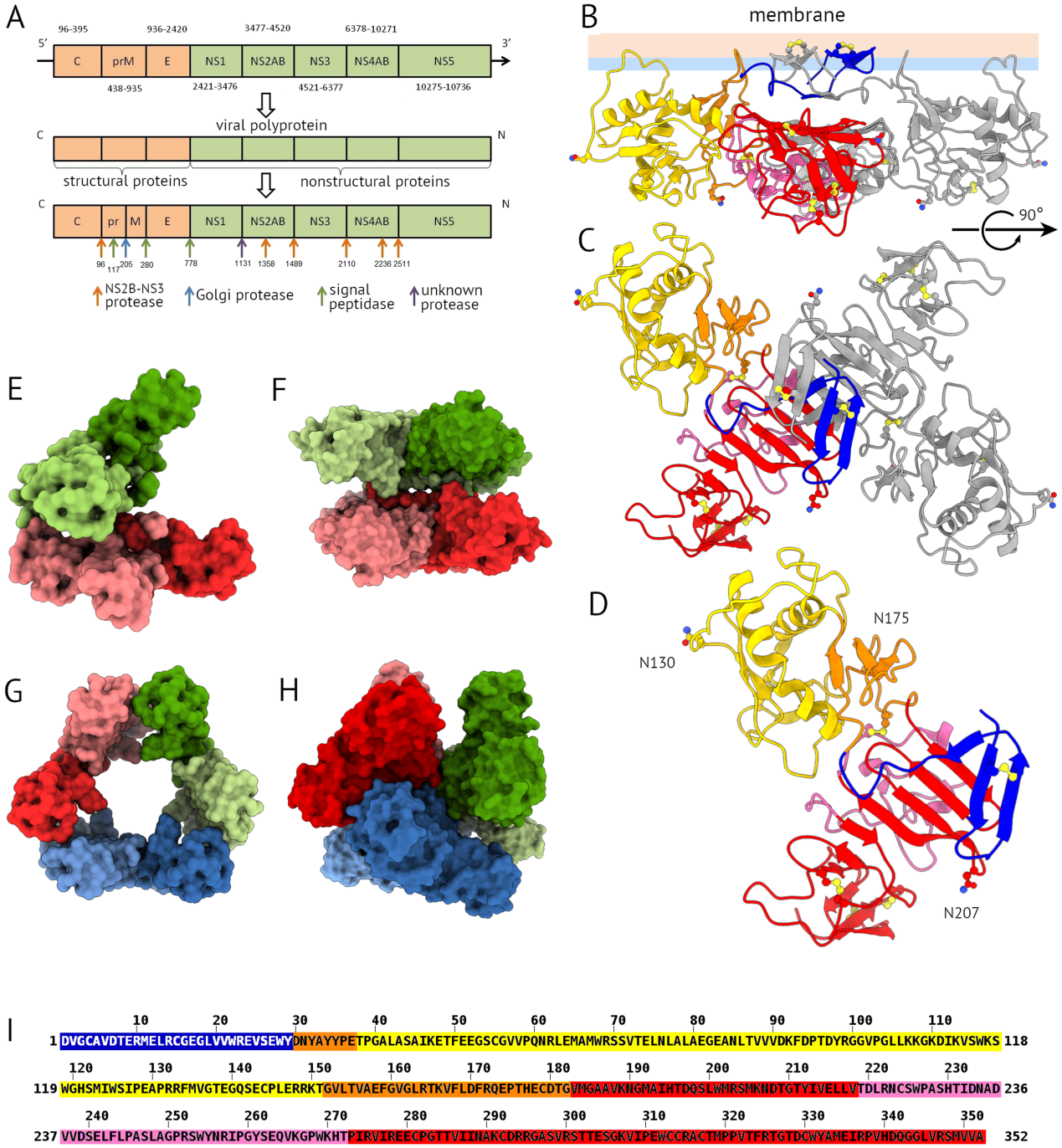


**Figure 1.** Genetic and structural basis of the orthoflavivirus NS1 protein. (**A**) – Scheme of the genome and polyprotein of orthoflaviviruses, numbering is given for the sequences of dengue virus serotype 1 (GenBank ID: U88536). (**B–D**) – The cryo-EM structure of NS1 (PDB ID 7WUS [24]): (**B**, **C**) – dimer, (**D**) – monomer. Color coding: β-barrel (residues 1–29) – blue, connector domain (residues 30–37, 152–182) – orange, α-helical wing (residues 38–151) – yellow, β-ladder (residues 183–352) – red, spaghetti loop (residues 219–272) – pink. Glycosylation sites – Asn130 and Asn270 (Asn175 is glycosylated in YFV) – are marked, disulfide bonds are shown as ball-and-stick models. (**E–H**) – Multimeric forms of the NS1 protein: (**E**) – "soft" tetramer (PDB ID 7WUU [24]), (**F**) – "stable" tetramer (PDB ID: 7WUT [24]), (**G**) – secreted "head-to-head" hexamer (PDB ID: 7WUV [24]), (**H**) – "side-to-side" hexamer (PDB ID: 8WBE [25]). (**I**) – NS1 protein sequence of TBEV strain Absettarov (GenBank KU885457.1), colored by protein domains. The color version of the figure is available in the electronic version of the article.

*Table 1.* Complete structures of NS1 protein in PDB

| PDB ID | Virus | Year | Method | Resolution, Å | Oligomeric state | Reference |
|---|---|---|---|---|---|---|
| 4O6D | WNV | 2014 | X-ray crystallography | 2.59 | Dimer | [28] |
| 4O6C | WNV | 2014 | X-ray crystallography | 2.75 | Dimer | [28] |
| 4TPL | WNV | 2014 | X-ray crystallography | 2.90 | Dimer | [32] |
| 4O6B | DENV2 | 2014 | X-ray crystallography | 3.00 | Dimer | [28] |
| 7WUS | DENV2 | 2022 | cryo-EM | 3.40 | Dimer | [24] |
| 7WUT | DENV2 | 2022 | cryo-EM | 3.50 | Tetramer | [24] |
| 7WUU | DENV2 | 2022 | cryo-EM | 8.00 | Tetramer | [24] |
| 7WUV | DENV2 | 2022 | cryo-EM | 8.30 | Tetramer | [24] |
| 7WUR | DENV2 | 2022 | cryo-EM | 3.50 | Dimer in complex with antibodies | [24] |
| 5K6K | ZIKV | 2016 | X-ray crystallography | 1.89 | Dimer | [33] |
| 5GS6 | ZIKV | 2016 | X-ray crystallography | 2.85 | Dimer | [34] |

in the infected organism: at the initial stage, NS1 is mainly present as a membrane-assosiated dimer (Fig. 1B,C). Subsequently, the protein is secreted into the blood as a tetramer, which exists in two forms — "soft" (Fig. 1E) and "stable" (Fig. 1F), or as a cyclic hexamer (Fig. 1G) with the internal cavity filled with lipids [24, 26]. In addition, a hexamer with a dense subunit packing was observed for recombinant NS1 proteins in certain expression conditions (Fig. 1H) [25]. The monomer structure contains four domains: the β-barrel, the connector domain, the α-wing, and the β-ladder (Fig. 1D) [27]. The surfaces of the β-barrel and the α-helical wing are hydrophobic and oriented inside the membranes or the lipid core of the hexamer, while the spaghetti loop (part of the β-ladder) is oriented outward [28]. The stabilization of multimers, as well as the interaction with the complement system proteins, are provided by complex glycans linked to Asn130 and Asn207 (as well as Asn175 in the YFV NS1) [28–31].

The availability of structural data allows to use docking as a tool for the search of potential ligands, and a sufficient number of structures enables us to use ensemble docking, which takes into account the conformational mobility of the protein by docking ligands into different structures of the same protein, thus improving the enrichment of the virtual screening results [35]. Previously, we developed a systematic ensemble docking method that incorporates all available structural information for a protein for structure-based virtual screening [36]. Since there is no structural information on either the TBEV NS1 protein or the interaction of small molecules with the orthoflavivirus NS1 protein in general, we performed homology modeling of TBEV NS1 and an analysis of NS1 structure to identify potential binding sites for small molecules. Based on the resulting set of models, we assessed the applicability of our systematic ensemble docking methodology to sets of protein structures that are heterogeneous in amino acid sequence.

## MATERIALS AND METHODS

### *Analysis of the Structure Data*

**Extraction of structural information.** The NS1 protein structures of flaviviruses (Supplementary Materials, Table ST1) were extracted from the PDB [37] by analyzing the search results for the query Full Text = "flavivirus NS1 protein" AND Parent Scientific Name (typically superkingdom or clade) = "Riboviria". To extract incorrectly annotated structures that were not identified by searching among the proteins of viruses of the genus *Orthoflavivirus*, the BLASTP program [38] was used, with the sequence of the NS1 protein of dengue virus serotype 1 (GenBank ID AAB70695) as a query. Thus, 2 structures were added to the set (PDB ID: 5O19, 5O36). The stereochemical quality of the structures was checked using the ProCheck web service [39].

**Spatial alignment of structures.** Spatial alignment was performed using VMD 1.9.3 [40]. To align dimeric structures, chains in PDB files were combined, then aligned by all $C_\alpha$ atoms of the combined chain, and then the chains were separated back using a Python 3.9 script.

After alignment, the pairwise root mean square deviation (RMSD) values of $C_\alpha$ atoms were calculated and visualized using the heat map method implemented in Python 3.9 using Pandas 1.4.1 [41], NumPy 1.21.6 [42], Matplotlib 3.5.1 [43], and seaborn 0.11.2 [44] libraries similar to the procedure described in [36].

### *Search for Potential Binding Sites of Small Molecules*

The search for pockets, i.e., cavities on the protein surface where specific binding of small molecules could occur, was performed for the monomer and dimer of the most diverse complete protein structures (4O6C, 4O6D, 5K6K, 5GS6) using two algorithmically different methods for identifying potential small molecule binding sites: FTSite (FTMap) [45–47] and

ProteinsPlus (DoGSiteScorer) [48, 49]. Both programs were used via a web interface. The outputs of the programs are sets of dots or spheres defining potential pockets. For the 4O6D and 5GS6 structures, the search for pockets was performed before and after removal of the polyhistidine tag, but the results did not differ, so its presence was not taken into account further.

FTSite implements an energy-based pocket search method. The search involves rigid docking of 16 small molecule probes and RMSD-based clusterisation of the results with cluster ranking based on the total number of interactions between the protein and all probes in the cluster.

The ProteinsPlus (DoGSiteScorer) algorithm is a geometric algorithm based on the molecular shape recognition method. A grid is generated around the protein molecule, and grid points are marked as occupied if they are within the van der Waals radius of any protein atom, and as unoccupied otherwise. Based on this markup, pockets large enough to accommodate at least one heavy atom are selected and ranked by volume. In the case of dimer analysis, we selected three pockets with the largest volumes and those symmetrical to them.

*Amino Acid Sequence Alignment and Homology Modeling*

Amino acid sequence alignment was performed using the MUSCLE web interface [50, 51]. The NS1 sequence of the TBEV strain Absettarov (GenBank KU885457.1) was used as the reference and sequences extracted from pdb files and NS1 protein sequences of epidemiologically significant orthoflaviviruses were included in the alignment (Supplementary Materials, Table ST3).

Homology modeling was performed using Modeller 10.5 [52]. Based on each individual template, 100 models were generated, and 300 models were also generated for all templates simultaneously. Models were scored with the DOPE and GA341 functions. Modeling was performed with implicit hydrogen atoms (automodel class). The "slow" optimization algorithm with a maximum number of iterations of 300 was used. Optimization was repeated twice. Since the optimized models had very large pairwise root mean square deviations (RMSD) upon the DOPE-based selection, the final model for comparison and docking was selected based on the lowest $C_\alpha$ atom RMSD from the 7WUS structure, which was the only crystal structure that did not contain unresolved regions (Supplementary Materials).

*Set of Diverse Compounds*

A set of 5000 diverse compounds was selected from a previously formed library of 20,000 diverse compounds [36] according to the following criteria: molecular weight from 200 Da to 400 Da, lipophilicity (clogP [53]) from -5 to 5, number of hydrogen bond donors no more than 5, number of hydrogen bond acceptors no more than 10, formal charge from -2 to 2, number of rotatable bonds no more than 8, number of heavy atoms from 15 to 50. A total of 9341 compounds passed the filtering, of which 5000 were selected based on diversity using the MaxMinPicker method [36].

*Ensemble Docking*

The docking pipeline was implemented using pyflare [54], a Python 3 library that allowed executing scripts for Flare 5.0.0, Cresset [55, 56]. Protein preparation (adding hydrogen atoms, assigning charges at pH 7.4) was performed using the proteinprep.py script. Docking into the prepared protein structure was performed using the docking.py script for each protein structure separately. The docking grid was generated at a distance of 6 Å from the ZINC000734046780 molecule (Supplementary Materials, Fig. SF1), manually placed using UCSF Chimera in the pocket between the β-barrel, β-ladder, and α-helical wing. Docking was performed with the "normal" quality parameter, corresponding to the standard docking algorithm implemented in the Lead Finder program [57]. The 5 highest ranked docking results by Rank score (a score optimized for correct energetic ranking of docking results for a specific molecule) were saved for each compound. The docking results were processed using Python 3.9 scripts. Scores were read from sdf files and the conformers with the highest Rank score were ranked based on the decrease in the VS score modulus (a score optimized for correct ranking of active molecules relative to inactive ones during virtual screening).

## RESULTS AND DISCUSSION

*Analysis of the Orthoflavivirus NS1 Protein Structure Data*

Since small molecule binding sites have not been described for the orthoflavivirus NS1 protein, we performed a comparative analysis of the available structures (Table 1) to identify potential binding sites by computational methods. Only 11 structures contain the complete amino acid sequence, two of them with insufficient resolution (7WUU, 7WUV), one (7WUT) in the form of a "stable tetramer" that contains an atypical β-barrel fold, and another one is the structure of a complex of the NS1 protein with antibodies (7WUR). The remaining structures represent only a part of the NS1 protein with a β-ladder and a spaghetti loop (listed in the Supplementary Materials, Table ST1 as the C-domain). The structures are characterized by high stereochemical quality: only a few residues are located in unfavorable areas of the Ramachandran plots, allowing us to conclude that the data are generally correct (Supplementary Materials, Table ST2).

Spatial alignment of monomers and dimers of the complete structures by RMSD of $C_\alpha$ atoms was performed for the purpose of comparative analysis, identification of conformational differences, and determination of the degree of symmetry of monomers in individual structures (Fig. 2, Supplementary Materials, Fig. SF2). For quantitative analysis of the alignment results, heat maps of pairwise RMSDs were constructed (Fig. 2).

All the structures are highly similar with low pairwise RMSD values: ≤1.4 Å in most cases. Such RMSD values are typical for structures of identical proteins and are explained by the resolution of the structures [58] and the overall flexibility of the polypeptide chains.

When aligning the complete structures, the most pronounced conformational differences are observed in the β-barrel region (residues 6–14) and in the loops of the α-helical wing. There are no noticeable differences in the relative positions of the monomers in the dimer of different structures. The high RMSD values for the 5GS6 and 5K6K structures are explained by deviations in the β-barrel region (5GS6-B, residues 6–14) and the α-helical wing (5GS6-B, A residues 62–82) (Supplementary Materials, Fig. SF3).

*Search for Potential Binding Sites for Small Molecules*

Based on the analysis of spatial alignment, as well as data on the completeness of resolution and stereochemical correctness of the structures, the most diverse and high-quality structures were selected to search for pockets on the protein surface: 4O6C (WNV), 4O6D (WNV), 5K6K (ZIKV), and 5GS6 (ZIKV). For more discussion on search results see Supplementary Materials.

Both programs reveal a pocket in the region of the dimerization interface between the β-barrel, connector domain, α-helical wing and β-ladder (Fig. 3A) formed by residues 1–15, 186–193, 202–207 of one chain and residues 1, 16–26, 156–162, 179–185, 193–200 of the other chain (Fig. 3B). In all structures, the pockets are lined mainly by hydrophilic residues, both donors and acceptors of hydrogen bonds. The hydrophobic side chains of the β-barrel residues are oriented outward from the pocket and form a hydrophobic surface that facilitates binding of the protein to membranes (Fig. 3C). Thus, the main chain atoms, also capable of forming hydrogen bonds, are accessible inside the pocket. This pocket was selected as a potential binding site for further virtual screening and analysis as the most conserved.

*Amino Acid Sequence Diversity of Epidemiologically Significant Orthoflaviviruses*

The amino acid sequences of epidemiologically significant orthoflaviviruses (Supplementary Materials, Table ST4) [59, 60] were obtained from the GenBank. For homology modeling, they were aligned with template sequences extracted from the NS1 protein structure files deposited in the RSCB PDB (PDB IDs: 4O6B, 4O6C, 4O6D, 4TPL, 5K6K, 5GS6, 7WUS). A separate alignment of the NS1 protein amino acid sequences of epidemiologically significant orthoflaviviruses was also performed against the NS1 protein sequence of the TBEV strain Absettarov (Supplementary Materials, Fig. SF4) to calculate the sequence homology matrix (Fig. 4). Based on this, tick-borne and mosquito-borne viruses can be divided into two groups with relatively low cross-similarity. The NS1 proteins of tick-borne viruses have high intergroup similarity, while the NS1 proteins

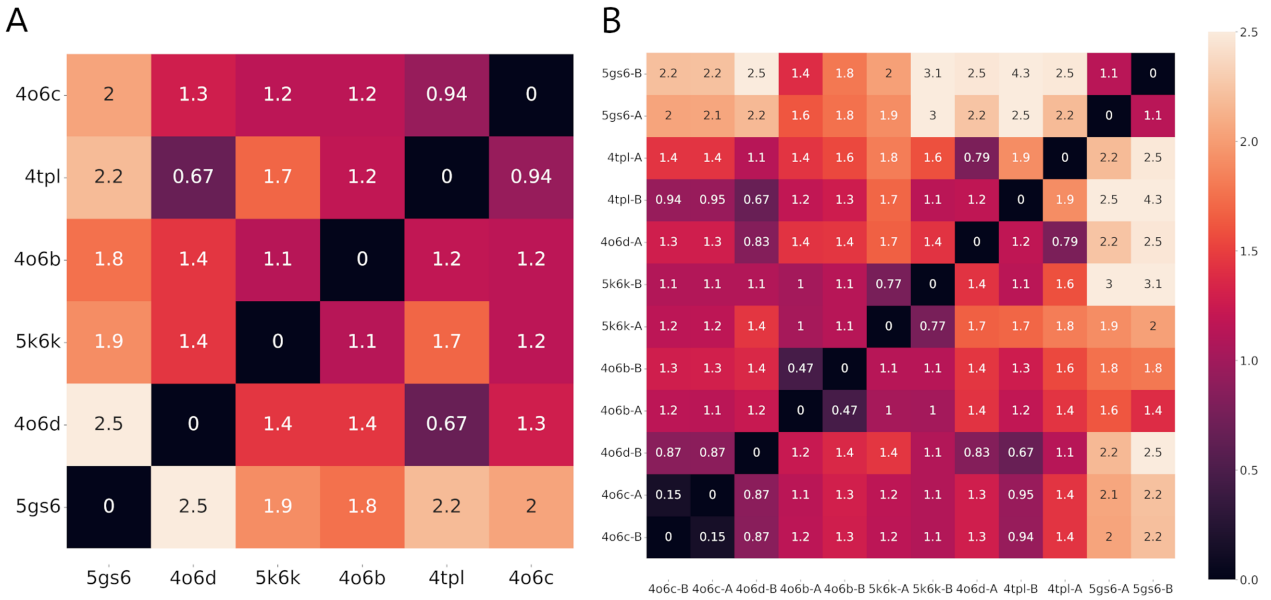


**Figure 2.** (**A**, **B**) – Heat maps of RMSD of $C_\alpha$ atoms of spatial alignment of (**A**) dimers and (**B**) monomers of complete structures of flavivirus NS1 protein. The color scale corresponds to RMSD values from 0 Å to 2.5 Å. The color version of the figure is available in the electronic version of the article.

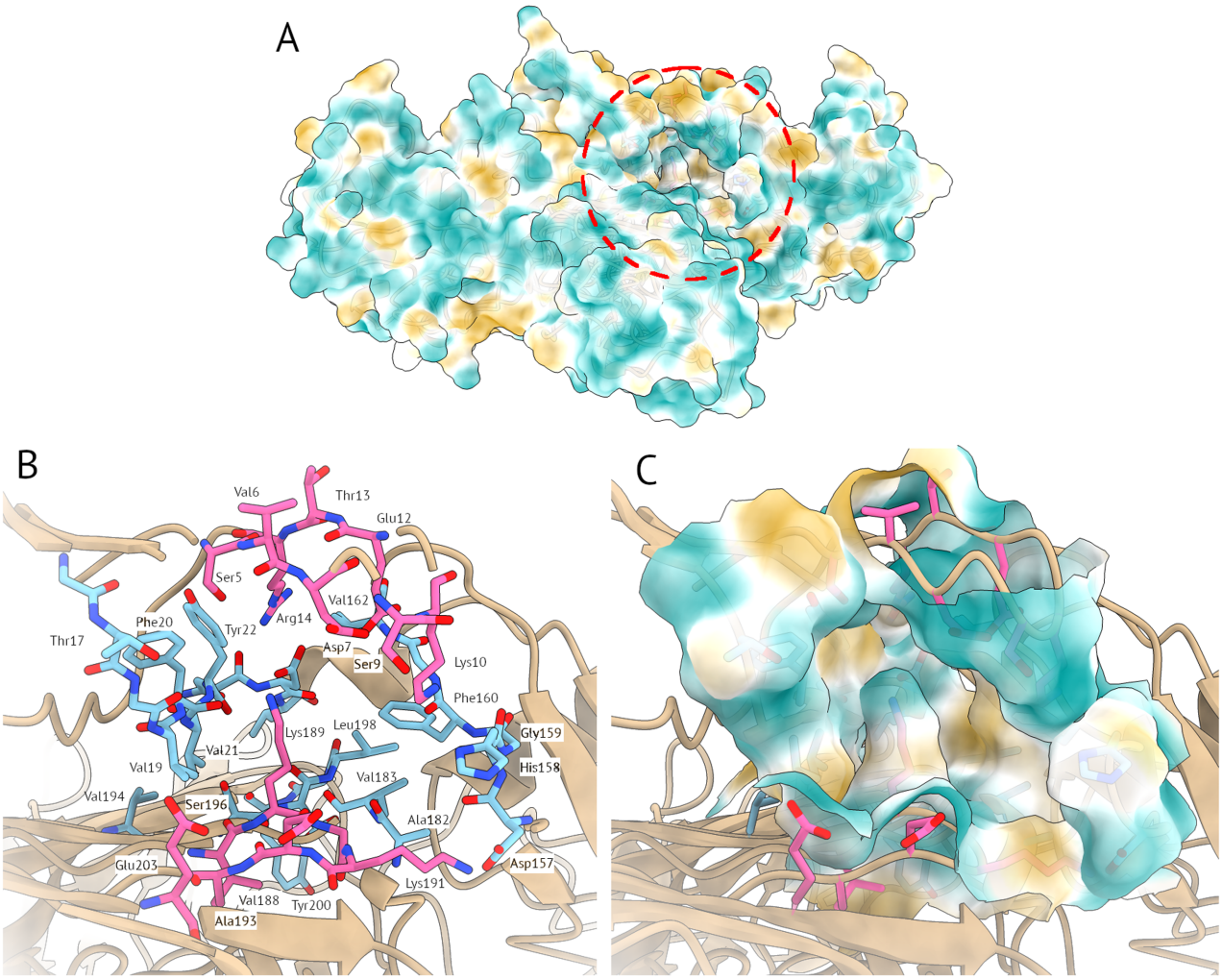


**Figure 3.** Potential small molecule binding site. (**A**) – Pocket location, (**B**) – residues forming the pocket, coloured by chain with chain A as pink and chain B as light blue, (**C**) – pocket surface, coloured by hydrophobicity with yellow depicting the high and cyan – low hydrophobicity. The color version of the figure is available in the electronic version of the article.

of mosquito-borne viruses are more diverse. As a consequence, the crystal structures available in the PDB may not be representative enough in the context of the diversity of NS1 protein sequences in orthoflaviviruses. Therefore, the reliability of the NS1 structure models of tick-borne orthoflaviviruses based on the available templates (Table 1) may be limited. Moreover, the existence of two distinct groups of NS1 sequences corresponding to the phylogenetic groups of the genus *Orthoflavivirus* may be sufficient to introduce selectivity of potential ligands against viruses with different vectors.

### *Homology Modeling of the Orthoflavivirus NS1 Protein Structure*

The models of the NS1 protein structure were generated using the Modeller 10.5 [61] by the homology modeling method using all complete dimeric NS1 structures available in the PDB (Table 1) as templates, individually and in combination (structure files deposited in Supplementary Materials). For further ensemble formation and virtual screening, we aimed to select one optimal model for each template and each virus. The standard selection criterion is based on the value of the DOPE scoring function [62], which is statistical in nature and prioritizes structures closest to the native state of the protein based on information on the probability density of interatomic distances. However, the optimal DOPE value in a series of models does not guarantee that the corresponding model would not have a significant conformational deviation from the template, particularly, in flexible regions. Since the DOPE values for all generated models were in the acceptable range and the differences between them were not significant (Supplementary Materials, Table ST3), the choice of the model for further study was made not by the DOPE value, but by the spatial alignment of all models with the 7WUS structure that does not contain unresolved regions. For each virus and each template, the models with the lowest RMSD of $C_\alpha$ atoms relative to 7WUS were selected.

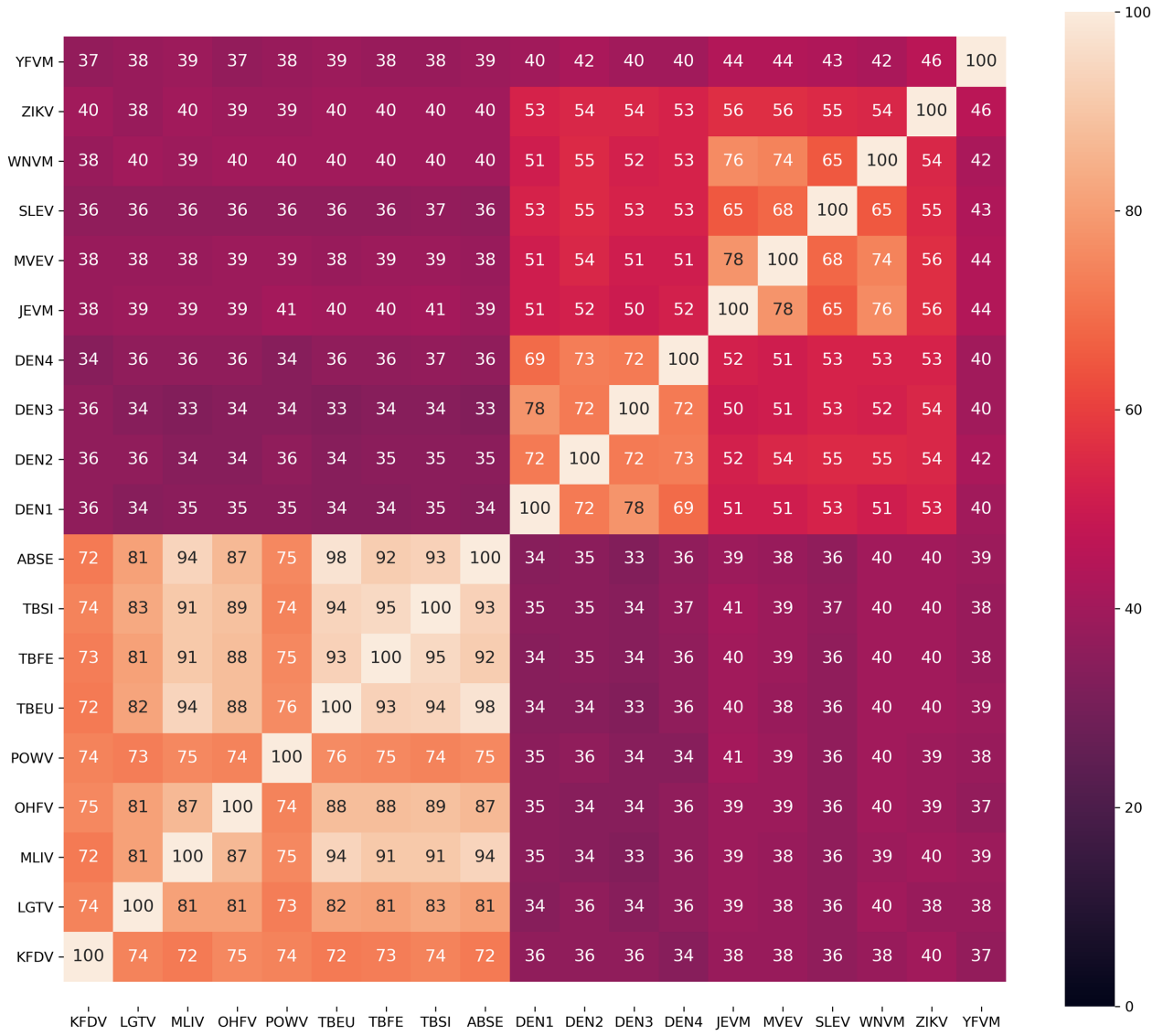


**Figure 4.** Homology matrix of amino acid sequences of the orthoflavivirus NS1 proteins. The abbreviations are explained in Supplementary Materials, Table ST3. The color version of the figure is available in the electronic version of the article.

In the framework of the previously described ensemble selection procedure [36], pairwise RMSDs of the $C_\alpha$ atoms of the residues forming the pocket in the dimerization interface region (V1–G15, A186–A193, E202–D207 of chain A and V1, T16–W26, D156–F162, D179–T185, V193–W200 of chain B) were calculated for all models. The selection of ensembles based on the diversity of conformations of the amino acid residues forming the potential binding site did not allow the formation of a representative ensemble of an acceptable size due to the very high conformational diversity of the generated coordinates: in a wide range of the threshold values for similarity and diversity of structures, only two models were selected for the ensemble.

Models based on the 4TPL structure have particularly high average RMSD values (Supplementary Materials, Fig. SF5, highlighted in orange). These models differ significantly from the others, which negatively affects the selection of the ensemble based on conformational diversity.

When considering the NS1 models of mosquito-borne viruses (Supplementary Materials, Fig. SF6) and tick-borne viruses (Supplementary Materials, Fig. SF7) separately, it is noticeable that the latter had a higher conformational diversity. In the case of models based on the same templates, the greatest conformational differences are observed for Powassan virus (POWV) and Kiasanur forest disease virus (KFDV), which have the lowest amino acid sequence similarity to both the NS1 proteins of other tick-borne viruses and the NS1 proteins of mosquito-borne viruses. In addition, the NS1 sequences of these viruses have multiple non-conservative substitutions in the region selected as a potential binding site

(Supplementary Materials, Fig. SF8). This questions the validity of modeling these proteins using the templates from mosquito-borne orthoflaviviruses.

At the next stage, principal component analysis (PCA) of the coordinates of the $C_\alpha$ atoms of residues forming the target pocket was performed (Fig. 5). The models based on the 4TPL template fall into a separate cluster, remote from the main set of models; this is consistent with the RMSD calculation results. At the same time, the 4TPL structure itself lies in the main cluster next to the other crystal structures (marked with crosses, Fig. 5). This is due to the fact that the 4TPL structure contains the longest unresolved region in the α-helical wing (residues 108–130) and the corresponding fragments of the protein are modeled stochastically. In this regard, the models based on the 4TPL template were not used further. The models based on the 4O6C and 5K6K templates are allocated to a separate cluster; however, upon visual analysis, no significant differences from the models based on other templates are observed in the generated structures. It should also be noted that the models built on the combined template lie in the projection on the principal components between the models built on the individual templates. Such "average" models have the highest similarity to all the others (Supplementary Materials, Fig. SF5, highlighted in blue), resulting in a low priority in the selection of an ensemble by diversity.

The POWV and KFDV NS1 models lie in principal component coordinates (Supplementary Materials, Fig. SF9) separately from the main clusters

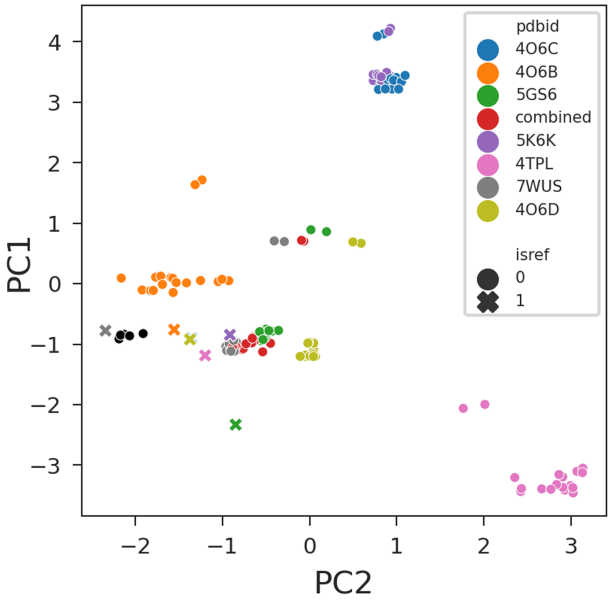


**Figure 5.** Principal component analysis of the coordinates of the $C_\alpha$ atoms of residues forming the target pocket of the orthoflavivirus NS1 protein for models and template structures. The models are colored by template. The "isref" category indicates whether the structure is a model or a template: models are shown as circles, templates as crosses. The color version of the figure is available in the electronic version of the article.

of models constructed using the same templates, while repeating the pattern of cluster arrangement. This is consistent with the low homology of their sequences with the other NS1 protein sequences. Thus it is reasonable to exclude such models from consideration for the selection of ensembles of protein structures, since they are not representative of the entire set of structures.

Removal of the models built using the 4TPL template and the POWV and KFDV NS1 protein models did not improve the ensemble selection results. Therefore, the systematic approach to ensemble selection based on the RMSD of binding site residues was abandoned.

*Comparison of Models by Ranking Ability*

As an alternative to the formation of an ensemble based on the protein structure, an approach based on the docking results was used. In this case, the conformational space of proteins is described implicitly based on the docking rank correlation: with a high correlation, the models are considered as virtually identical; with a low correlation, the models should belong to fundamentally different ensembles, and models with intermediate values of the correlation coefficient may be used for consensus ranking. To compare the ranking ability of the models, a library of diverse drug-like compounds from ZINC15 was docked into the pocket in the dimerization interface of all generated models and PDB structures using the Flare program. The docking results were ranked based on the scores from the VS score function. The correlation between pairwise RMSD, amino acid sequence homology, and the rank-order correlation coefficient was analyzed. On general consideration of all structure pairs, no clear correlation between these parameters is observed (Fig. 6, Supplementary Materials, Fig. SF10, 11); however, pairwise rank correlation coefficients do not exceed 0.739. Therefore, the available models are conformationally different enough for consensus ranking. For example, the three models with the highest sum of rank correlation coefficients, 2,188, can be selected as an ensemble: DENV4 NS1 model on 4O6C template, JEV NS1 model on 5K6K template, and Louping ill virus NS1 model on 5GS6 template (Fig. 7A). This ensemble provides a sustainable ranking, includes viruses transmitted by both ticks and mosquitoes and may be used to search for broad-spectrum ligands. Ensembles of four or more structures can be composed in a similar manner.

When considering pairs of models based on identical templates, three groups are distinguished with RMSD in the range from 0 to 2, from 2 to 4, and from 4 to 6, and within each group, structures with greater similarity of amino acid sequences could be expected to have lower RMSDs, but structural similarity has no significant effect on the ranking (Fig. 6B).

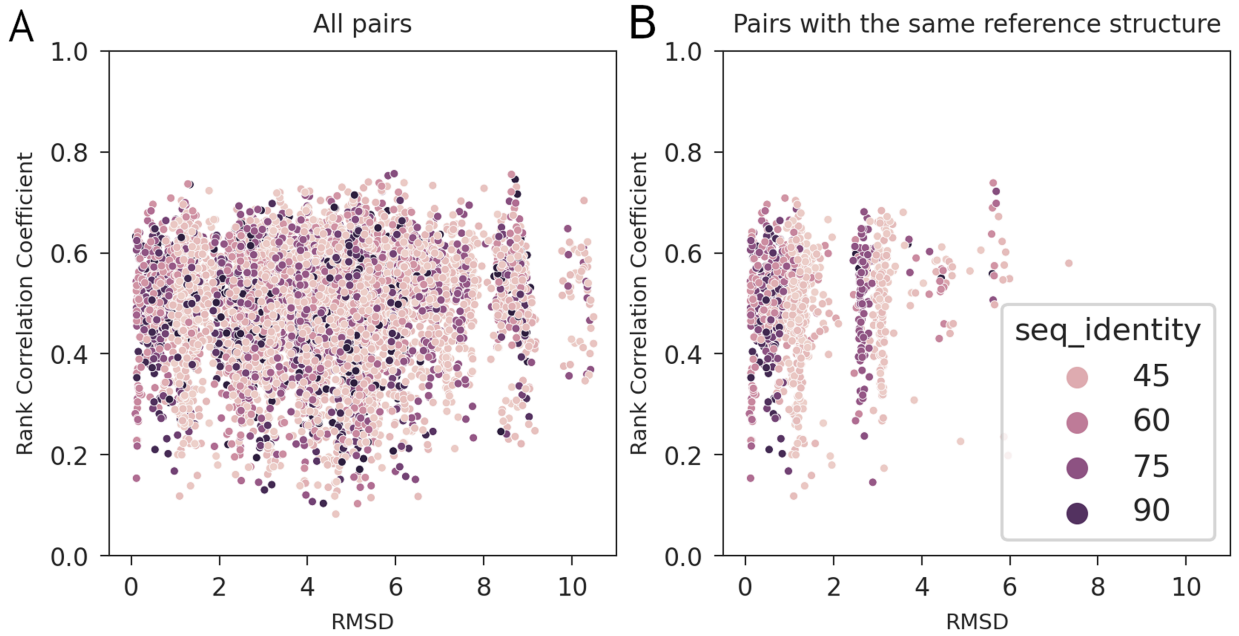


**Figure 6.** Dependence of the pairwise correlation coefficient of the docking ranks for the structures of orthoflavivirus NS1 models on the pairwise RMSD between the corresponding structures, colored by the percentage of similarity between the corresponding sequences. (**A**) For all pairs of structures, (**B**) for pairs of models of different proteins with the same template. The color version of the figure is available in the electronic version of the article.

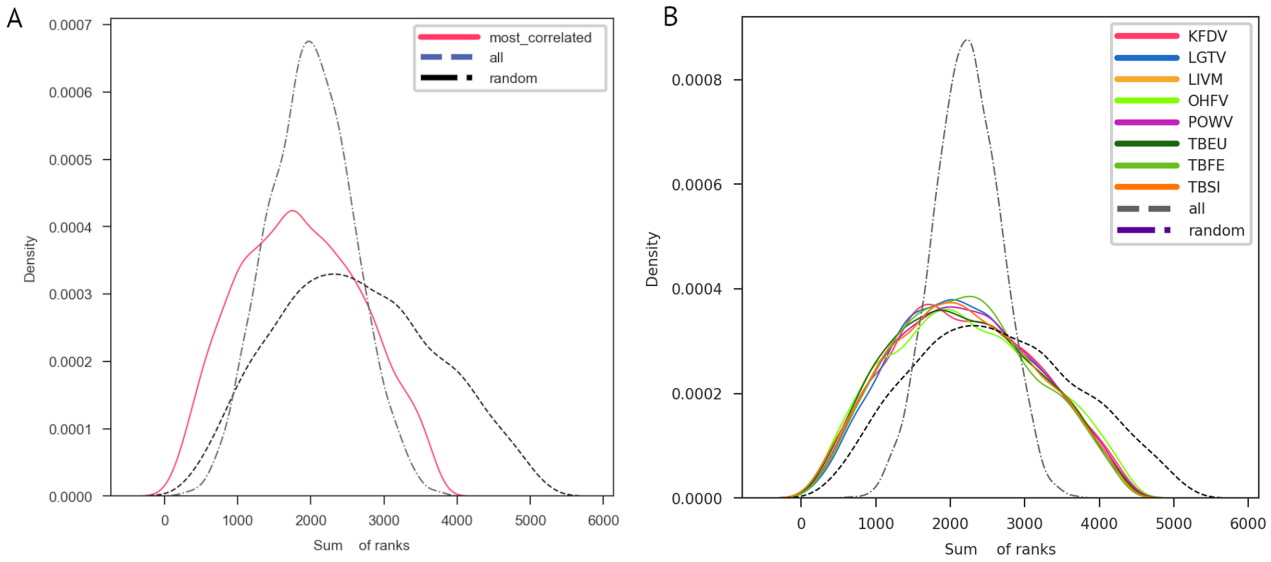


**Figure 7.** Distribution of the sum of docking ranks. (**A**) Normalized sum over the ensemble composed of DENV4 NS1 model on 4O6C template, JEV NS1 model on 5K6K template, and Louping ill virus NS1 model on 5GS6 template. (**B**) Normalized sum over the models of the NS1 protein for a single virus (for tick-borne viruses). The color version of the figure is available in the electronic version of the article.

When analyzing the distributions of docking scores (Supplementary Materials, Fig. SF12–14), no correlation was found for the median, minimum, and maximum score values vs. the template structure and amino acid sequence. This is consistent with other results confirming the high contribution of stochastic coordinate generation in homology modeling. In such a situation, it is natural to use the sum of ranks for the ensemble as a consensus score. The analysis of the distribution of the sum of ranks was carried out for ensembles based on a shared template or sequence in order to identify possible patterns associated with the difference in the NS1 sequences of both individual viruses and those grouped by vectors. The distribution of the normalized sum of ranks for ensembles of models constructed using one template and one virus (Fig. 7B) has a single-peaked asymmetric shape. For comparison, the distributions of the sum of randomly

generated ranks and the sum of ranks for all models were calculated. All considered ensembles of models led to distributions wider than the sum of random ranks, demonstrating their ability to prioritize molecules better than random models. Also, in ensembles consisting of 7 NS1 models of one virus based on different templates, the shoulder in the region of small sums of ranks is located to the left from the distribution of the sum of ranks for all models. This means that the same molecules are consensusly-prioritized in the docking results for such small ensembles.

The distributions of the normalized sum of ranks for the ensembles of NS1 models of different viruses for each template separately and the ensembles of NS1 models of individual viruses for all templates were compared using the Kolmogorov-Smirnov test (Supplementary Materials, Table ST5). The comparison allows us to reject the hypothesis about the identity of the distributions of the normalized sum of ranks for each vector separately and for all viruses. At the same time, for the ensembles of NS1 proteins derived from viruses with the same vector, the number of molecules with a normalized sum of ranks ≤500 (potential hits of virtual screening) is greater than for the ensembles including NS1 proteins of all the studied viruses (Supplementary Materials, Table ST6). Thus, the separation of mosquito- and tick-borne viruses when constructing ensembles should be considered as an effective strategy for the screening of low-molecular compounds for experimental research.

## CONCLUSION

The orthoflavivirus NS1 protein is relatively understudied as a drug target, although it is attractive due to low homology to human proteins and importance for the replication process. Based on limited available structure information, we employed homology modeling for generating inputs for ensemble docking and analyzed the influence of heterogeneity of these models on the ranking ability of structure-based virtual screening. Ranking-based ensemble selection led to more consistent ensembles than RMSD-based selection. Forming an ensemble based on ranking of diverse compounds corroborated the diversity of models and allowed to select ones providing an acceptable similarity for consensus ranking of potential broad-spectrum NS1 ligands. Further combining models into ensembles based on a template protein or a target virus led to ensembles that ranked compounds better than a random selection. Combining NS1 structures from viruses with different vectors in one ensemble negatively affected the virtual screening enrichment of potential specific NS1 ligands. The ensembles demonstrated the ability to prioritize some groups of compounds over random ones, thus being suitable for virtual screening of potential NS1 ligands.

## FUNDING

Chumakov FSC R&D IBP RAS (Institute of Poliomyelitis) fundamental research assignment FNZG-2024-0005.

## COMPLIANCE WITH ETHICAL STANDARDS

This article does not contain any research involving humans or the use of animals as objects.

## CONFLICT OF INTEREST

The authors declare no conflicts of interest.

## REFERENCES

1. *Pierson T.C., Diamond M.S.* (2020) The continued threat of emerging flaviviruses. Nat. Microbiol., **5**(6), 796–812. DOI: 10.1038/s41564-020-0714-0
2. *Pustijanac E., Buršić M., Talapko J., Škrlec I., Meštrović T., Lišnjić D.* (2023) Tick-borne encephalitis virus: A comprehensive review of transmission, pathogenesis, epidemiology, clinical manifestations, diagnosis, and prevention. Microorganisms, **11**(7), 1634. DOI: 10.3390/microorganisms11071634
3. *Kolyasnikova N.M., Ishmukhametov A.A., Akimkin V.G.* (2023) The current state of the problem of tick-borne encephalitis in Russia and the world. Epidemiology and Vaccinal Prevention., **22**(1), 104–123. DOI: 10.31631/2073-3046-2023-22-1-104-123
4. *Putintseva E.V., Udovichenko S.K., Nikitin D.N., Boroday N.V., Baturin A.A., Machneva A.Yu., Antonov A.S., Zarubin N.A., Toporkov A.V.* (2023) West Nile fever in the Russian Federation in 2022, the incidence forecast for 2023. Problems of Particularly Dangerous Infections, 1, 75–84. DOI: 10.21055/0370-1069-2023-1-75-84
5. *Ruzek D., Avšič Županc T., Borde J., Chrdle A., Eyer L., Karganova G., Kholodilov I., Knap N., Kozlovskaya L., Matveev A., Miller A.D., Osolodkin D.I., Överby A.K., Tikunova N., Tkachev S., Zajkowska J.* (2019) Tick-borne encephalitis in Europe and Russia: Review of pathogenesis, clinical features, therapy, and vaccines. Antiviral Res., **164**, 23–51. DOI: 10.1016/j.antiviral.2019.01.014
6. *Redoni M., Yacoub S., Rivino L., Giacobbe D.R., Luzzati R., di Bella S.* (2020) Dengue: Status of current and under-development vaccines. Rev. Med. Virol., **30**(4), e2101. DOI: 10.1002/rmv.2101
7. *Staples J.E., Monath T.P., Gershman M.D., Barrett A.D.T.* (2017) Yellow fever vaccines. In: Plotkin's Vaccines, Elsevier, pp. 1181–1265.e20. DOI: 10.1016/B978-0-323-35761-6.00063-8
8. *Yun S.-I., Lee Y.-M.* (2014) Japanese encephalitis: The virus and vaccines. Hum. Vaccin. Immunother., **10**(2), 263–279. DOI: 10.4161/hv.26902
9. *Morrone S.R., Lok S.-M.* (2019) Structural perspectives of antibody-dependent enhancement of infection of dengue virus. Curr. Opin. Virol., **36**, 1–8. DOI: 10.1016/j.coviro.2019.02.002

10. *Bardina S.V., Bunduc P., Tripathi S., Duehr J., Frere J.J., Brown J.A., Nachbagauer R., Foster G.A., Krysztof D., Tortorella D., Stramer S.L., García-Sastre A., Krammer F., Lim J.K.* (2017) Enhancement of Zika virus pathogenesis by preexisting antiflavivirus immunity. Science, **356**(6334), 175–180. DOI: 10.1126/science.aal4365
11. *Santos-Peral A., Luppa F., Goresch S., Nikolova E., Zaucha M., Lehmann L., Dahlstroem F., Karimzadeh H., Thorn-Seshold J., Winheim E., Schuster E.-M., Dobler G., Hoelscher M., Kümmerer B.M., Endres S., Schober K., Krug A.B., Pritsch M., Barba-Spaeth G., Rothenfusser S.* (2024) Prior flavivirus immunity skews the yellow fever vaccine response to cross-reactive antibodies with potential to enhance dengue virus infection. Nat. Commun., **15**(1), 1696. DOI: 10.1038/s41467-024-45806-x
12. *Chong H.Y., Leow C.Y., Abdul Majeed A.B., Leow C.H.* (2019) Flavivirus infection — A review of immunopathogenesis, immunological response, and immunodiagnosis. Virus Res., **274**, 197770. DOI: 10.1016/j.virusres.2019.197770
13. *Rastogi M., Singh S.K.* (2020) Zika virus NS1 affects the junctional integrity of human brain microvascular endothelial cells. Biochimie, **176**, 52–61. DOI: 10.1016/j.biochi.2020.06.011
14. *Puerta-Guardo H., Glasner D.R., Espinosa D.A., Biering S.B., Patana M., Ratnasiri K., Wang C., Beatty P.R., Harris E.* (2019) Flavivirus NS1 triggers tissue-specific vascular endothelial dysfunction reflecting disease tropism. Cell Rep., **26**(6), 1598–1613.e8. DOI: 10.1016/j.celrep.2019.01.036
15. *Puerta-Guardo H., Glasner D.R., Harris E.* (2016) Dengue virus NS1 disrupts the endothelial glycocalyx, leading to hyperpermeability. PLOS Pathogens, **12**(7), e1005738. DOI: 10.1371/journal.ppat.1005738
16. *Avirutnan P., Fuchs A., Hauhart R.E., Somnuke P., Youn S., Diamond M.S., Atkinson J.P.* (2010) Antagonism of the complement component C4 by flavivirus nonstructural protein NS1. J. Exp. Med., **207**(4), 793–806. DOI: 10.1084/jem.20092545
17. *Chen S., Wu Z., Wang M., Cheng A.* (2017) Innate immune evasion mediated by flaviviridae non-structural proteins. Viruses, **9**(10), 291. DOI: 10.3390/v9100291.
18. *Bílý T., Palus M., Eyer L., Elsterová J., Vancová M., Růžek D.* (2015) Electron tomography analysis of tick-borne encephalitis virus infection in human neurons. Sci. Rep., **5**(1), 10745. DOI: 10.1038/srep10745
19. *Płaszczyca A., Scaturro P., Neufeldt C.J., Cortese M., Cerikan B., Ferla S., Brancale A., Pichlmair A., Bartenschlager R.* (2019) A novel interaction between dengue virus nonstructural protein 1 and the NS4A-2K-4B precursor is required for viral RNA replication but not for formation of the membranous replication organelle. PLOS Pathogens., **15**(5), e1007736. DOI: 10.1371/journal.ppat.1007736
20. *de Silva A.M., Rey F.A., Young P.R., Hilgenfeld R., Vasudevan S.G.* (2018) Viral entry and NS1 as potential antiviral drug targets. Adv. Exp. Med. Biol., **1062**, 107–113. DOI: 10.1007/978-981-10-8727-1_8
21. *Songprakhon P., Thaingtamtanha T., Limjindaporn T., Puttikhunt C., Srisawat C., Luangaram P., Dechtawewat T., Uthaipibull C., Thongsima S., Yenchitsomanus P.-T., Malasit P., Noisakran S.* (2020) Peptides targeting dengue viral nonstructural protein 1 inhibit dengue virus production. Sci. Rep., **10**(1), 12933. DOI: 10.1038/s41598-020-69515-9
22. *Raza S., Abbas G., Azam S.S.* (2020) Screening pipeline for flavivirus based inhibitors for Zika virus NS1. IEEE/ACM Trans. Comput. Biol. Bioinform., **17**(5), 1751–1761. DOI: 10.1109/TCBB.2019.2911081
23. *Modhiran N., Gandhi N.S., Wimmer N., Cheung S., Stacey K., Young P.R., Ferro V., Watterson D.* (2019) Dual targeting of dengue virus virions and NS1 protein with the heparan sulfate mimic PG545. Antiviral Res., **168**, 121–127. DOI: 10.1016/j.antiviral.2019.05.004
24. *Shu B., Ooi J.S.G., Tan A.W.K., Ng T.-S., Dejnirattisai W., Mongkolsapaya J., Fibriansah G., Shi J., Kostyuchenko V.A., Screaton G.R., Lok S.-M.* (2022) CryoEM structures of the multimeric secreted NS1, a major factor for dengue hemorrhagic fever. Nat. Commun., **13**(1), 6756. DOI: 10.1038/s41467-022-34415-1
25. *Pan Q., Jiao H., Zhang W., Chen Q., Zhang G., Yu J., Zhao W., Hu H.* (2024) The step-by-step assembly mechanism of secreted flavivirus NS1 tetramer and hexamer captured at atomic resolution. Sci. Adv., **10**(18), eadm8275. DOI: 10.1126/sciadv.adm8275
26. *Gutsche I., Coulibaly F., Voss J.E., Salmon J., d'Alayer J., Ermonval M., Larquet E., Charneau P., Krey T., Mégret F., Guittet E., Rey F.A., Flamand M.* (2011) Secreted dengue virus nonstructural protein NS1 is an atypical barrel-shaped high-density lipoprotein. Proc. Natl. Acad. Sci. USA, **108**(19), 8003–8008. DOI: 10.1073/pnas.1017338108
27. *Roy P., Roy S., Sengupta N.* (2020) Disulfide reduction allosterically destabilizes the β-ladder subdomain assembly within the NS1 dimer of ZIKV. Biophys. J., **119**(8), 1525–1537. DOI: 10.1016/j.bpj.2020.08.036
28. *Akey D.L., Brown W.C., Dutta S., Konwerski J., Jose J., Jurkiw T.J., del Proposto J., Ogata C.M., Skiniotis G., Kuhn R.J., Smith J.L.* (2014) Flavivirus NS1 structures reveal surfaces for associations with membranes and the immune system. Science, **343**(6173), 881–885. DOI: 10.1126/science.1247749
29. *Zhang S., Wang X., He Y., Hu T., Guo J., Wang M., Jia R., Zhu D., Liu M., Zhao X., Yang Q., Wu Y., Zhang S., Huang J., Mao S., Ou X., Gao Q., Sun D., Liu Y., Zhang L., Chen S., Cheng A.* (2021) N130, N175 and N207 are N-linked glycosylation sites of duck tembusu virus NS1 that are important for viral multiplication, viremia and virulence in ducklings. Vet. Microbiol., **261**, 109215. DOI: 10.1016/j.vetmic.2021.109215
30. *Somnuke P., Hauhart R.E., Atkinson J.P., Diamond M.S., Avirutnan P.* (2011) N-Linked glycosylation of dengue virus NS1 protein modulates secretion, cell-surface expression, hexamer stability, and interactions with human complement. Virology, **413**(2), 253–264. DOI: 10.1016/j.virol.2011.02.022
31. *Pryor M.J., Wright P.J.* (1994) Glycosylation mutants of dengue virus NS1 protein. J. Gen. Virol., **75**(Pt 5), 1183–1187. DOI: 10.1099/0022-1317-75-5-1183
32. *Akey D.L., Brown W.C., Konwerski J.R., Ogata C.M., Smith J.L.* (2014) Use of massively multiple merged data for low-resolution S-SAD phasing and refinement of flavivirus NS1. Acta Cryst. D., **70**(10), 2719–2729. DOI: 10.1107/S1399004714017556
33. *Brown W.C., Akey D.L., Konwerski J.R., Tarrasch J.T., Skiniotis G., Kuhn R.J., Smith J.L.* (2016) Extended surface for membrane association in Zika virus NS1 structure. Nat. Struct. Mol. Biol., **23**(9), 865–867. DOI: 10.1038/nsmb.3268
34. *Xu X., Song H., Qi J., Liu Y., Wang H., Su C., Shi Y., Gao G.F.* (2016) Contribution of intertwined loop to membrane association revealed by Zika virus full-length NS1 structure. EMBO J., **35**(20), 2170–2178. DOI: 10.15252/embj.201695290
35. *Carlson H.A., Masukawa K.M., McCammon J.A.* (1999) Method for including the dynamic fluctuations of a protein in computer-aided drug design. J. Phys. Chem. A, **103**(49), 10213–10219. DOI: 10.1021/jp991997z

36. *Fomina A.D., Uvarova V.I., Kozlovskaya L.I., Palyulin V.A., Osolodkin D.I., Ishmukhametov A.A.* (2024) Ensemble docking based virtual screening of SARS-CoV-2 main protease inhibitors. Mol. Inf., **43**(8), e202300279. DOI: 10.1002/minf.202300279
37. *Berman H.M., Westbrook J., Feng Z., Gilliland G., Bhat T.N., Weissig H., Shindyalov I.N., Bourne P.E.* (2000) The Protein Data Bank. Nucleic Acids Res., **28**(1), 235–242. DOI: 10.1093/nar/28.1.235
38. *Boratyn G.M., Thierry-Mieg J., Thierry-Mieg D., Busby B., Madden T.L.* (2019) Magic-BLAST, an accurate RNA-Seq aligner for long and short reads. BMC Bioinformatics, **20**(1), 405. DOI: 10.1186/s12859-019-2996-x
39. *Laskowski R.A., MacArthur M.W., Moss D.S., Thornton J.M.* (1993) PROCHECK: A program to check the stereochemical quality of protein structures. J. Appl. Crystallogr., **26**(2), 283–291. DOI: 10.1107/S0021889892009944
40. *Humphrey W., Dalke A., Schulten K.* (1996) VMD: Visual molecular dynamics. J. Mol. Graph., **14**(1), 33–38. DOI: 10.1016/0263-7855(96)00018-5
41. *McKinney W.* (2010) Data structures for statistical computing in Python. Proceedings of the 9th Python in Science Conference, 56–61. DOI: 10.25080/Majora-92bf1922-00a
42. *Harris C.R., Millman K.J., van der Walt S.J., Gommers R., Virtanen P., Cournapeau D., Wieser E., Taylor J., Berg S., Smith N.J., Kern R., Picus M., Hoyer S., van Kerkwijk M.H., Brett M., Haldane A., del Río J.F., Wiebe M., Peterson P., Gérard-Marchant P., Sheppard K., Reddy, T., Weckesser W., Abbasi H., Gohlke C., Oliphant T.E.* (2020) Array programming with NumPy. Nature, **585**(7825), 357–362. DOI: 10.1038/s41586-020-2649-2
43. *Hunter J.D.* (2007) Matplotlib: A 2D graphics environment. Comput. Sci. Eng., **9**(3), 90–95. DOI: 10.1109/MCSE.2007.55
44. *Waskom M.L.* (2021) Seaborn: Statistical data visualization. J. Open Source Softw., **6**(60), 3021. DOI: 10.21105/joss.03021
45. *Ngan C.-H., Hall D.R., Zerbe B., Grove L.E., Kozakov D., Vajda S.* (2012) FTSite: High accuracy detection of ligand binding sites on unbound protein structures. Bioinformatics, **28**(2), 286–287. DOI: 10.1093/bioinformatics/btr651
46. *Kozakov D., Grove L.E., Hall D.R., Bohnuud T., Mottarella S.E., Luo L., Xia B., Beglov D., Vajda S.* (2015) The FTMap family of web servers for determining and characterizing ligand-binding hot spots of proteins. Nat. Protoc., **10**(5), 733–755. DOI: 10.1038/nprot.2015.043
47. Retrieved January 15, 2020 from https://ftsite.bu.edu/
48. *Volkamer A., Griewel A., Grombacher T., Rarey M.* (2010) Analyzing the topology of active sites: On the prediction of pockets and subpockets. J. Chem. Inf. Model., **50**(11), 2041–2052. DOI: 10.1021/ci100241y
49. Zentrum für Bioinformatik: Universität Hamburg — Proteins Plus Server. Retrieved January 15, 2020 from https://proteins.plus/
50. *Edgar R.C.* (2004) MUSCLE: Multiple sequence alignment with high accuracy and high throughput. Nucleic Acids Res., **32**(5), 1792–1797. DOI: 10.1093/nar/gkh340
51. Retrieved August 08, 2023 from https://www.ebi.ac.uk/Tools/msa/muscle/
52. *Webb B., Sali A.* (2016) Comparative protein structure modeling using MODELLER. Curr. Protoc. Bioinformatics, **54**, 5.6.1–5.6.37. DOI: 10.1002/cpbi.3
53. *Wildman S.A., Crippen G.M.* (1999) Prediction of physicochemical parameters by atomic contributions. J. Chem. Inf. Comput. Sci., **39**(5), 868–873. DOI: 10.1021/ci9903071
54. Cresset/flare-python-pyflare GitLab. GitLab. Retrieved August 20, 2023 from https://gitlab.com/cresset/flare-python-pyflare
55. Ligand and structure-based drug design software | Flare. Retrieved October 01, 2024 from https://www.cresset-group.com/software/flare/
56. *Bauer M.R., Mackey M.D.* (2019) Electrostatic complementarity as a fast and effective tool to optimize binding and selectivity of protein-ligand complexes. J. Med. Chem., **62**(6), 3036–3050. DOI: 10.1021/acs.jmedchem.8b01925
57. *Stroganov O.V., Novikov F.N., Stroylov V.S., Kulkov V., Chilov G.G.* (2008) Lead Finder: An approach to improve accuracy of protein-ligand docking, binding energy estimation, and virtual screening. J. Chem. Inf. Model., **48**(12), 2371–2385. DOI: 10.1021/ci800166p
58. *Kufareva I., Abagyan R.* (2012) Methods of protein structure comparison. Methods Mol. Biol., **857**, 231–257. DOI: 10.1007/978-1-61779-588-6_10
59. Retrieved October 01, 2024 from https://ictv.global/report/chapter/flaviviridae/flaviviridae/orthoflavivirus
60. *Walker P.J., Siddell S.G., Lefkowitz E.J., Mushegian A.R., Adriaenssens E.M., Alfenas-Zerbini P., Dempsey D.M., Dutilh B.E., García M.L., Curtis Hendrickson R., Junglen S., Krupovic M., Kuhn J.H., Lambert A.J., Łobocka M., Oksanen H.M., Orton R.J., Robertson D.L., Rubino L., Sabanadzovic S., Simmonds P., Smith D.B., Suzuki N., van Doorslaer K., Vandamme A.-M., Varsani A., Zerbini F.M.* (2022) Recent changes to virus taxonomy ratified by the international committee on taxonomy of viruses. Arch. Virol., **167**(11), 2429–2440. DOI: 10.1007/s00705-022-05516-5
61. *Fiser A., Sali A.* (2003) Modeller: Generation and refinement of homology-based protein structure models. Methods Enzymol., **374**, 461–491. DOI: 10.1016/S0076-6879(03)74020-8
62. *Shen M., Sali A.* (2006) Statistical potential for assessment and prediction of protein structures. Prot. Sci., **15**(11), 2507–2624. DOI: 10.1110/ps.062416606

Received: 16. 10. 2024.
Revised: 28. 10. 2024.
Accepted: 05. 11. 2024.

# МОДЕЛИРОВАНИЕ СТРУКТУРЫ БЕЛКА NS1 ОРТОФЛАВИВИРУСОВ ПО ГОМОЛОГИИ ДЛЯ ВИРТУАЛЬНОГО СКРИНИНГА ПОТЕНЦИАЛЬНЫХ ЛИГАНДОВ

***А.Д. Фомина[1,2], В.А. Палюлин[2], Д.И. Осолодкин[1,3]****

[1]Федеральный научный центр исследований и разработки
иммунобиологических препаратов имени М.П. Чумакова РАН (Институт полиомиелита),
108819, поселение Московский, посёлок Института полиомиелита, домовладение 8, корп. 1, Москва;
*эл. почта: osolodkin_di@chumakovs.su
[2]Химический факультет Московского государственного университета имени М.В. Ломоносова, Москва
[3]Институт трансляционной медицины и биотехнологии, Первый московский государственный
медицинский университет имени И.М. Сеченова Минздрава России, Москва

Белок NS1 ортофлавивирусов является относительно малоизученной мишенью для разработки противоортофлавивирусных препаратов широкого спектра действия. В настоящее время не опубликованы структуры белка NS1 ортофлавивирусов, переносимых клещами, однако эти структуры можно моделировать по гомологии, генерируя таким образом большое количество структурной информации. Нами было проведено моделирование по гомологии структур белка NS1 эпидемиологически значимых ортофлавивирусов и анализ возможности использования этих моделей для виртуального скрининга методом ансамблевого докинга. Были показаны ограничения метода и важность разделения моделей на основании организма-переносчика при отборе ансамбля.

*Полный текст статьи на русском языке доступен на сайте журнала (http://pbmc.ibmc.msk.ru).*

**Ключевые слова:** ортофлавивирусы; белок NS1; ансамблевый докинг; моделирование по гомологии

**Финансирование.** Работа выполнена в рамках государственного задания FNZG-2024-0005.

Поступила в редакцию: 16.10.2024; после доработки: 28.10.2024; принята к печати: 05.11.2024.